Hydroxylated *Closo*-Dodecaborates $M_2B_{12}(OH)_{12}$ (M = Li, Na, K and Cs); Structural Analysis, Thermal Properties and Solid-State Ionic Conductivity.

Mathias Jørgensen[1,2], Steffen R.H. Jensen[1,2], Terry D. Humphries[1], Matthew R. Rowles[3], Maria V. Sofianos[4], Craig E. Buckley[1], Torben R. Jensen[2], Mark Paskevicius[1*]*

1. Department of Physics and Astronomy, Fuels and Energy Technology Institute, Curtin University, GPO Box U1987, Perth, WA 6845, Australia.

2. Center for Materials Crystallography, Interdisciplinary Nanoscience Center (iNANO), Department of Chemistry, Aarhus University, Langelandsgade 140, DK-8000 Aarhus, Denmark.

3. John de Laeter Centre, Curtin University, GPO Box U1987, Perth, WA 6845, Australia.

4. School of Chemical and Bioprocess Engineering, University College Dublin, Belfield, Dublin 4, Ireland.

Ion conductivity; batteries; crystal structure; thermal properties; boranes; borates

Closo-borates and derivative thereof have shown great potential as electrolyte materials for all-solid-state batteries owing to their exceptional ionic conductivity and high thermal and chemical stability. However, because of the myriad of possible chemical modifications of the large, complex anion, only a fraction of *closo*-borate derivatives has so far been investigated as electrolyte materials. Here, the crystal structures, thermal properties, and ionic conductivities of $M_2B_{12}(OH)_{12}$ (M = Li, Na, K and Cs) are investigated with a focus on their possible utilization as new solid-state ion conductors for solid-state batteries. The compounds generally show rich thermal polymorphism, with eight identified polymorphs among the four dehydrated compounds. Both $Li_2B_{12}(OH)_{12}$ and $Na_2B_{12}(OH)_{12}$ undergo a first order transition, in which the cation sub-lattices become disordered, resulting in an order of magnitude jump in ionic conductivity for $Na_2B_{12}(OH)_{12}$. $K_2B_{12}(OH)_{12}$ undergoes a second order polymorphic transition driven by a change in the anion-cation interaction, with no evidence of dynamic disorder. The ionic conductivities of $M_2B_{12}(OH)_{12}$ range from $1.60 \cdot 10^{-8}$ to $5.97 \cdot 10^{-5}$ S cm^{-1} at 250 °C for M = Cs and Li, respectively, showing decreasing conductivity with increasing cation size. Compared with the analogous $M_2B_{12}H_{12}$ compounds, such relatively low conductivities are suggested to be a consequence of strong and directional anion-cation interactions resulting in a more static anion framework.

Introduction

In the modern world, batteries are an essential part of our everyday life. Common battery technologies are based on liquid electrolytes, owing to their high ionic conductivity and the maturity of the technology. However, such electrolytes are often based on flammable organic liquids, which can be hazardous if the battery is punctured or overcharged.[1] Another concern

with lithium ion batteries is the limited amount of lithium available in the worlds crust, and the fact that Li from Li-batteries is challenging to recycle, resulting in potentially increasing energy storage costs.[2] Instead of using lithium, cheaper alkali and alkaline earth metals (*e.g.* sodium, potassium, or magnesium) are also being considered for battery applications. Increased energy densities in the batteries could be achieved by utilizing pure metal anodes if the liquid electrolyte is exchanged with a solid electrolyte in order to limit hazardous dendrite formation. In recent years, many advances have been made in the area of solid-state electrolytes, especially for lithium ion batteries.[3,4] A range of new solid-state lithium ion conductors have been discovered, such as $Li_{10}GeP_2S_{12}$[5] and garnet[6] based materials, which show impressive ionic conductivities in the order of 10^{-3} to 10^{-2} S cm^{-1} at room temperature (RT), rivalling conductivities of liquid electrolytes. State-of-the-art solid-state electrolytes for sodium batteries include Na-β-Al_2O_3,[7] which is currently used as a solid-state electrolyte in high temperature Na–S batteries, while polycrystalline $K_2Fe_4O_7$ shows the highest conductivity for potassium, with an ionic conductivity of 5.0×10^{-2} S cm^{-1} at RT.[8]

Lithium ion conduction was recently discovered in complex metal hydrides, which are now considered as battery materials.[9–15] The advantages of hydride based materials are their low densities and relatively high electrochemical stability. In some cases, the solids have flexible structures owing to a versatile coordination environment of the complex anion, which lead to the discovery of a new cation conductivity mechanism observed for both $LiBH_4 \cdot 0.5NH_3$ and $Mg(BH_4)_2 \cdot NH_3$.[16,17] Recently, focus was also directed towards higher borates, such as *closo*-borates.[3,18,19] Higher borates were first synthesized in the 1950s and 60s, where the stable *closo*-dodecaborate anion, $[B_{12}H_{12}]^{2-}$, was observed,[20] however, their potential as solid-state electrolytes were only recently realised.[3] For example, $Na_2B_{12}H_{12}$ shows ionic conductivities of

approximately 0.1 S cm^{-1} above an order-disorder polymorphic transition (255 °C).[21] An interest in reducing the transition temperature to below RT has led to investigations of mixed anion compounds and the effect of chemically modifying the complex anion. For example, halogenation of the *closo*-borate cage has been shown for $Na_2B_{12}X_{12}$ (X = F, Cl, Br, and I), where the transition temperature was increased,[22,23] while carbon substitution in the boron cage, resulted in a significant lowering of the transition temperature.[18,24]

In order to gain further insight into the influence of the chemical modification of *closo*-borates on the order-disorder polymorphic transition and the ionic conductivity, we here present a study of the electrolyte properties of $M_2B_{12}(OH)_{12}$ (M = Li, Na, K, and Cs). These compounds were chosen to investigate the physical, structural and ionic conductivity differences between the hydroxylated compounds and their hydrogenous analogues, $M_2B_{12}H_{12}$. The expectation was that changes in anion charge distribution would impact the ionic conductivity behavior of the cation. The compounds are characterized by *in-situ* synchrotron radiation (SR-PXD) and electrochemical impedance spectroscopy (EIS) to investigate the correlation between structure, polymorphism, and ionic conductivity. Furthermore, the influence of hydrogen bonds between the more complex anions on the disorder transition temperature is investigated.

Experimental

Synthesis

The synthesis of $Cs_2B_{12}(OH)_{12}$ was adapted from earlier work.[25] $Cs_2B_{12}H_{12}$ (Strem, 98%) was dissolved in 27 % H_2O_2 (Alfa Aesar) and heated to reflux behind a blast shield. After 5 days at reflux, additional portions (4 - 20 mL) of H_2O_2 were added to the solution (after cooling to below 40 °C) every second day. To monitor the reaction progress ^{11}B NMR spectroscopy was

conducted on aliquots of the solution. Once full conversion to $Cs_2B_{12}(OH)_{12}$ was observed, the reaction mixture was further refluxed until the peroxide content was < 1 ppm, followed by removal of the solvent by rotary evaporation. **Caution: This entire process is dangerous as explosive peroxides could form. As such, the solution was carefully monitored so that it never reached dryness during reflux and a blast shield was in place at all times.**

Cation exchange was conducted by dissolving $Cs_2B_{12}(OH)_{12}$ in hot (60 °C) milliQ water, followed by the addition of aqueous *M*Cl in excess (*M* = Li, Na and K). The white precipitate, $M_2B_{12}(OH)_{12}$, was filtered and dried under dynamic vacuum at room temperature. $Li_2B_{12}(OH)_{12}$, $Na_2B_{12}(OH)_{12}$, and $Cs_2B_{12}(OH)_{12}$ were further dried under dynamic vacuum at 210, 150 and 190 °C, respectively, for 24 hours. $K_2B_{12}(OH)_{12}$ did not require further treatment. Based on Rietveld refinement of the structural models of the compounds (vide infra), there is no evidence of significant Cs^+ incorporation in the precipitated products, at least in a crystalline form. A summary of samples is shown in Table 1.

Table 1: Overview of synthesized products.

Sample name	Product	Synthesis	Analysis
Li1	$Li_2B_{12}(OH)_{12}{\cdot}xH_2O$	Ion exchange of Cs1	*in-situ* SR-PXD, DSC-TGA-MS
Li2	$Li_2B_{12}(OH)_{12}$	Heat treatment of Li1 at 210 °C	*in-situ* SR-PXD, FTIR, PXD, EIS
Na1	$Na_2B_{12}(OH)_{12}{\cdot}4H_2O$	Ion exchange of Cs1	*in-situ* SR-PXD
Na2	$Na_2B_{12}(OH)_{12}$	Heat treatment Na1 at 150 °C	FTIR, PXD, DSC-TGA-MS, EIS
K1	$K_2B_{12}(OH)_{12}$	Ion exchange of Cs1	*in-situ* SR-PXD, DSC-TGA-MS, PXD, EIS
Cs1	$Cs_2B_{12}(OH)_{12}{\cdot}2H_2O$	$Cs_2B_{12}H_{12} + H_2O_2$ for 28 days	^{11}B NMR, *in-situ* SR-PXD
Cs2	$Cs_2B_{12}(OH)_{12}$	Heat treatment of Cs1 at 190 °C	FTIR, EIS, DSC-TGA-MS

Characterization

Nuclear magnetic resonance (NMR) spectra were collected in D_2O on a Bruker Avance III 400 MHz spectrometer (400.1 MHz for ^{1}H; 128.4 MHz for ^{11}B). ^{11}B (proton decoupled) spectra were referenced to $OEt_2 \cdot BF_3$.

Fourier transform infrared (FTIR) spectroscopy was undertaken on powder samples on a Perkin Elmer Spectrum 100 in attenuated total reflection (ATR) mode after brief (< 10 s) air exposure.

Differential scanning calorimetry (DSC) and thermogravimetric analysis (TGA) were performed using a Perkin Elmer STA 6000 apparatus simultaneously with mass spectrometry (MS) analysis of the residual gases using a Hiden Analytical HPR-20 QMS sampling system. The samples (~ 7 mg) were placed in an Al_2O_3 crucible and heated from 30 to 400 °C (5 °C/min) in an argon flow of 40 mL/min. Cyclic DSC-TGA was also performed on a Mettler Toledo DSC 1 with heating/cooling rates of 10 °C/min under an argon flow of 20 mL/min.

Electrochemical impedance spectroscopy (EIS) was measured using a BioLogic MTZ-35 impedance analyzer with a high-temperature sample holder. The samples were pressed into pellets with a thickness of ~1 mm and 6.35 mm in diameter. The measurements were conducted in an Argon atmosphere with a K-type thermocouple 5 mm from the sample. The impedance data were measured at 500 mV AC from 1 - 10^6 Hz. To derive the ionic conductivity (σ) from the impedance data the *x*-intercept of the Nyquist impedance plot was determined using a known method.[22]

Laboratory X-ray powder diffraction (PXD) was measured on a Rigaku Smart Lab diffractometer using a Cu source and convergent beam focusing in a capillary setup (Cu $K_{\alpha 1}$

radiation, λ = 1.54056 Å). Data was collected in the 2θ range of 5° to 60° with 2°/min using D/tex detector. The samples were packed in borosilicate (0.5 mm inner diameter) capillaries and sealed under argon inside a glovebox using glue.

In-situ synchrotron radiation powder diffraction (SR-PXD) data for samples Li1, Na1, K1 and Cs1 were obtained on the Powder Diffraction (PD) beam line at the Australian Synchrotron using a Mythen strip detector at λ = 0.8263076 Å. Samples were packed in borosilicate capillaries (0.7 mm inner diameter) and sealed in a gas cell under an argon atmosphere and were heated to T > 500 °C using a hot air blower at 5 °C/min. *In-situ* SR-PXD of Li1 was obtained at the BM01A beam line at the European Synchrotron Radiation Facility (ESRF) using a Dectris Pilatus 2M detector at λ = 0.68663 Å.[26] The sample was sealed in a quartz capillaries (0.5 mm inner diameter) under an argon atmosphere and heated to T > 500 °C using a hot air blower at 10 °C/min.

Unit cells were indexed in the program FOX using the integrated volume dichotomy algorithm,[27] utilizing *in-situ* SR-PXD data to distinguish different polymorphs and compounds. The structures were then solved in the same program, using a real space parallel tempering Monte Carlo method. A rigid body of $[B_{12}(O)_{12}]$ (without H due to the low scattering power), based on previous studies,[28] was used throughout the structure determination process. Final Rietveld refinements were performed in FullProf retaining the rigid body, except for the model of β-$K_2B_{12}(OH)_{12}$ where oxygen was refined freely after convergence of the rigid body refinement.[29] Furthermore, for the models of γ-$Li_2B_{12}(OH)_{12}$ and β-$Na_2B_{12}(OH)_{12}$ soft constraints were utilized for the B–O distance.

Results and discussion

Synthesis of hydroxylated *closo*-dodecaborates

The synthesis of cesium dodecahydroxy-*closo*-dodecaborate, $Cs_2B_{12}(OH)_{12}$, from $Cs_2B_{12}H_{12}$ was followed by ^{11}B (proton decoupled) NMR spectroscopy (Figure 1), where the spectra evolved during substitution of H^- by OH^-. Initially, resonances at –35, –32 and –15 ppm were observed, identical to those reported previously,[28] although after 28 days of reaction these merged into a single resonance at –18 ppm, which corresponds to the hydroxylated *closo*-borate anion, $[B_{12}(OH)_{12}]^{2-}$. PXD of Cs1 confirms the formation of $Cs_2B_{12}(OH)_{12}\cdot 2H_2O$ (Figure S1),[28] along with a second phase, which was identified as a different polymorph of $Cs_2B_{12}(OH)_{12}\cdot 2H_2O$ (*vide infra*).

Cation exchange to form $Li_2B_{12}(OH)_{12}$, $Na_2B_{12}(OH)_{12}$, and $K_2B_{12}(OH)_{12}$ from aqueous solutions of $Cs_2B_{12}(OH)_{12}$ and chloride salts, was confirmed by their insolubility in water (compared to the soluble reagents) and by their unique diffraction patterns (samples Li1, Na1 and K1, Figures S2, S3 and S4, respectively). The diffractograms of $Na_2B_{12}(OH)_{12}\cdot 4H_2O$ and $K_2B_{12}(OH)_{12}$ were identified based on previous work, while the structure of hydrated $Li_2B_{12}(OH)_{12}$ has not previously been reported.

The coordinated water from Cs1, Li1, and Na1 was removed by thermal treatment at 210, 150 and 190 °C, respectively, under dynamic vacuum followed by analysis using FTIR spectroscopy (Figure S5). The absence of the H–O–H bending mode at 1650 cm^{-1} confirmed dehydration, while the absence of B–H stretching (2500 cm^{-1}) or bending (1050 cm^{-1}) modes confirmed the complete hydroxylation of the anion, in addition to NMR results.

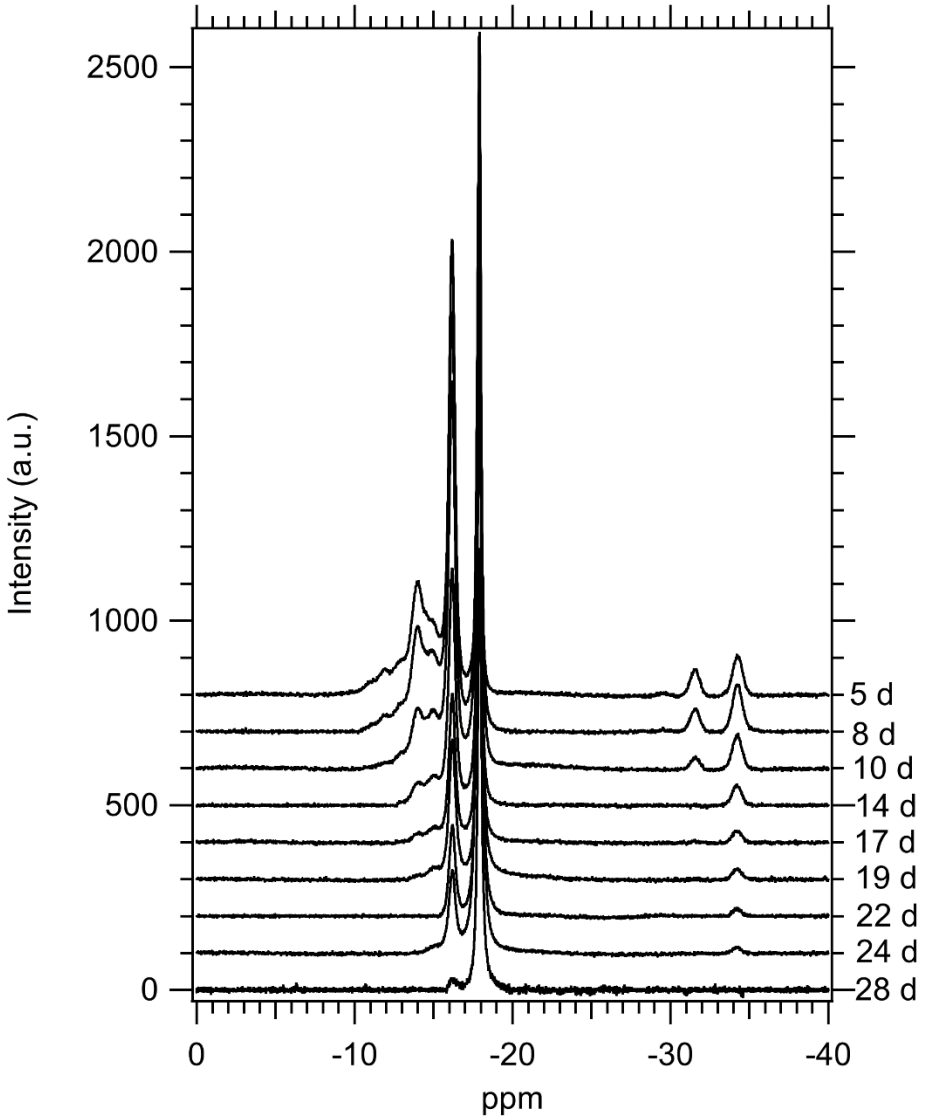

Figure 1: ^{11}B (proton decoupled) NMR of $Cs_2B_{12}(OH)_{12}$ during the 28 day synthesis.

Crystal structures and thermal stability

Lithium hydroxylated closo-dodecaborate

The *in-situ* SR-PXD data of sample Li1 reveal the presence of at least two different phases at RT (Figure 2a). One is suggested to be an impurity, possibly carried over from the synthesis of $Cs_2B_{12}(OH)_{12}$. The diffraction peaks from this phase disappear at around 220 °C, which is in

agreement with a minor mass loss observed in the TGA data (Figure S6). The other set of diffraction peaks is suggested to belong to a hydrate of $Li_2B_{12}(OH)_{12}$. Interestingly, this phase was not achieved in future syntheses (Figures S2 and S7), which could indicate a meta-stable structure. At ~140 °C these peaks disappear, while diffraction peaks from what has been identified as a monohydrate, based on TGA measurements (Figure S8a), appear. Unfortunately, because of the low crystallinity of the sample, peak overlap, and the presence of unidentified peaks in the diffractograms, neither of the two presumed hydrates of $Li_2B_{12}(OH)_{12}$ could be indexed. At 220 °C the last remnant of water is removed (in agreement with TGA data), resulting in the appearance of peaks belonging to α-$Li_2B_{12}(OH)_{12}$. The structure is expected to be monoclinic as no higher symmetry could be indexed, however, a unit cell could not reliably be determined due to the poor crystallinity of the sample. At ~300 °C a transition from α-$Li_2B_{12}(OH)_{12}$ to β-$Li_2B_{12}(OH)_{12}$ is observed. Again, the data did not allow for a detailed structure determination, though an orthorhombic unit cell with lattice constants a = 12.087(2), b = 12.087(3), and c = 8.516(2) Å (approximately corresponding to a $\sqrt{2}c \times \sqrt{2}c \times c$ unit cell) and space group *Pnnn* (No. 48) corresponds reasonably well to the observed diffraction data (Figure S9) and suggests that the anion is positioned on a body-centered sublattice, with side lengths close to an ideal BCC packing (8.516(2) – 8.544(2) Å).

Another polymorphic transition is observed at 490 °C, increasing symmetry to a cubic unit cell with symmetry $Im\bar{3}$ (No. 204) and lattice parameter a = 8.5707(2) Å (γ-$Li_2B_{12}(OH)_{12}$) (Figure S10). Surprisingly, there is no evidence of disorder of the anion lattice (Figure 2b) as otherwise seen for most other metal *closo*-borates. However, the cations are best described by both linear (8*c* Wyckoff site) and octahedral sites (6*b* Wyckoff site) (relative to the anion), indicating disorder in the cation sublattice. It should be noted that the positions of weakly scattering Li^+

was challenging to determine from X-ray data and carries some uncertainty. According to the model, the linearly coordinated Li^+ are octahedrally coordinated relative to O with Li−O distances of 2.259(3) Å, while the octahedrally coordinated Li^+ has a fourfold planar coordination relative to O with a Li–O distance of 2.317(1) Å. The latter coordination intuitively appears less stable relative to the linear coordination, though occupancy refinement suggests that it has a higher occupancy (~65 % of Li^+ situated in this site). It is possible that the octahedral sites, situated on the unit cell faces, are in fact split into two sites (12*e* Wyckoff site) akin to the sodium analogue (*vide infra*), giving rise to a trigonal prismatic coordination, however, upon refinement this position showed significant distortion of the coordination, thus the Li^+-ion was kept in the 6*b* Wyckoff position.

Based on the known structures of $M_2B_{12}(OH)_{12}$ and derivatives,[28] hydrogen bonds among the anions are expected to stabilize the structure. Interestingly, based on O−O distances in γ-$Li_2B_{12}(OH)_{12}$ (shortest distance 3.084(3) Å, compared with a combined van der Waals radius of 3.04 Å) there is no evidence of strong hydrogen bonds between different anion cages. Thus, hydrogen bonds are not expected to be responsible for suppressing anion reorientational disorder.

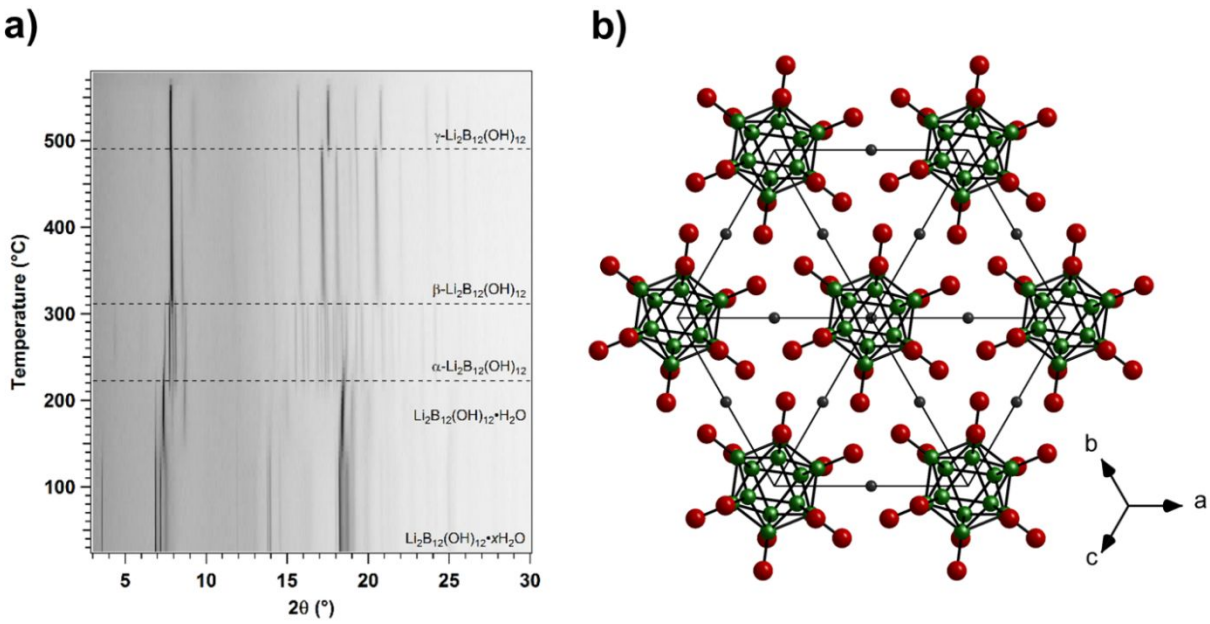

Figure 2: (a) *In-situ* synchrotron radiation powder X-ray diffraction of $Li_2B_{12}(OH)_{12}$ (Li1) heated from RT to 580 °C ($\Delta T/\Delta t$ = 5 °C/min, λ = 0.8263076 Å; (b) Crystal structure of the γ-polymorph of $Li_2B_{12}(OH)_{12}$. Li atoms are shown as grey spheres; O atoms as red spheres; B as green spheres; hydrogen atoms were not modelled and are thus not shown.

Sodium hydroxylated closo-dodecaborate

The *in-situ* SR-PXD data of sample Na1 reveal reflections from $Na_2B_{12}(OH)_{12}{\cdot}4H_2O$ (Figure 3a),[28] as well as a second minor phase with similar features to the unknown phase of the Li1 sample. In this sample, the peaks from the unknown phase disappear at ~100 °C, significantly lower than the 220 °C observed in the Li1 sample, indicating that the impurity depends on the metal chloride added during synthesis. At 80 °C the diffraction intensity from $Na_2B_{12}(OH)_{12}{\cdot}4H_2O$ disappears and is replaced by a new diffraction pattern showing significant peak broadening. The new peaks are suggested to belong to dehydrated $Na_2B_{12}(OH)_{12}$, denoted

α-$Na_2B_{12}(OH)_{12}$, based on the TGA results (Figure S8b). Due to the poor crystallinity of the sample it was not possible to index the α-polymorph.

Above 270 °C another polymorphic transition occurs, in which the Bragg reflections become sharper, but remain in similar 2θ positions indicating structural similarities between the two polymorphs. This phase is denoted β-$Na_2B_{12}(OH)_{12}$ and crystallizes in a cubic unit cell with space group $Im\bar{3}$ (No. 204) and lattice constant a = 8.6291(3) Å at T = 288 °C (Figures 3b and S11). As is the case for γ-$Li_2B_{12}(OH)_{12}$, there is no evidence of disorder of the anion. Owing to the higher scattering power of Na^+, the cation positions could be determined with more certainty than for Li^+. Again, the cation sublattice is disordered, with Na^+ partially occupying tetrahedral sites (relative to the anions) in the 12*e* Wyckoff position. Relative to oxygen, the coordination is trigonal prismatic with Na–O distances ranging from 2.415(5) to 2.530(3) Å. Similar to γ-$Li_2B_{12}(OH)_{12}$, a minimum O–O distance of 3.146(4) Å suggests only weak hydrogen bonds may be present in the structure.

While the temperature of the polymorphic transition to β-$Na_2B_{12}(OH)_{12}$ (270 °C) is similar to that of the α– to β–$Na_2B_{12}H_{12}$ transition (~255 °C),[21] the transitions are not directly comparable since the transition in $Na_2B_{12}H_{12}$ involves an onset of anion dynamics as well as cation dynamics. Above 550 °C the diffraction from $Na_2B_{12}(OH)_{12}$ disappears indicating decomposition of the compound, which is significantly later than what is observed from TGA-DSC (Figure S12).

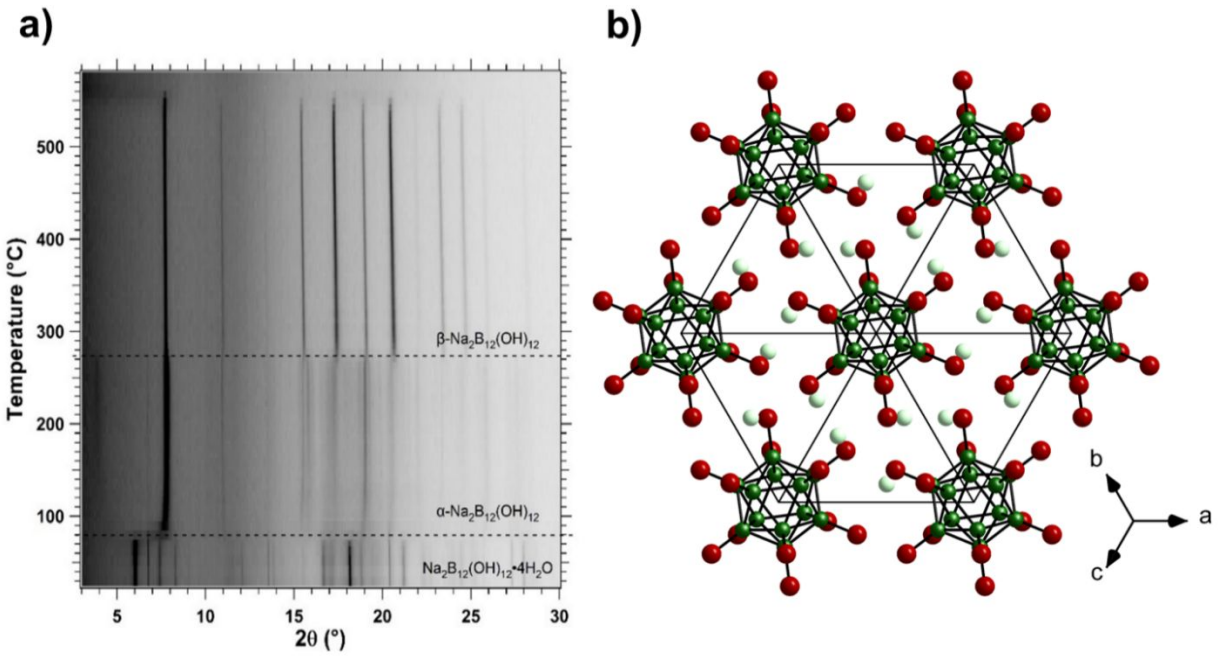

Figure 3: (a) *In-situ* synchrotron radiation powder X-ray diffraction of $Na_2B_{12}(OH)_{12}\cdot 4H_2O$ (Na1) heated from RT to 580 °C ($\Delta T/\Delta t$ = 5 °C/min, λ = 0.8263076 Å); (b) Crystal structure of the β-polymorph of $Na_2B_{12}(OH)_{12}$. Na atoms are shown as light green spheres; O atoms as red spheres; B as green spheres; hydrogen atoms were not modelled and are thus not shown.

Potassium hydroxylated closo-dodecaborate

In-situ SR-PXD data of K1 at RT reveal the water-free $K_2B_{12}(OH)_{12}$ compound with space group $P2_1/n$ (No. 14) and lattice parameters of a = 7.186(1), b = 10.263(7), c = 8.956(3) Å, and β = 93.64(1)° (Figure 4a).[28] A subset of Bragg reflections from α-$K_2B_{12}(OH)_{12}$ begins to merge around 230 °C, which is reminiscent of a second order polymorphic transition, however, from the indexing there is no evidence of a change in the crystal symmetry. Interestingly, an onset of mass loss is observed at this temperature (Figure S8c), which is concomitant with a water signal in the mass spectrometry (MS) data (Figure S13c). However, based on sequential refinement of the *in-situ* SR-PXD data, there is no decrease in the unit cell volume, and refinement of the

oxygen occupancy does not suggest that the hydroxyl groups on the boron cages are released in the form of water. It is possible that the water release is from the surface of the powder, though judging from the release temperature, the coordination must be exceptionally strong. Further merging of Bragg reflections occurs immediately after the first merge, at ~430 °C, which is caused by a second order polymorphic transition, resulting in an increase in symmetry to an orthorhombic unit cell with space group *Pnnm* (No. 58, a super group of $P2_1/n$) and lattice parameters a = 7.3559(1), b = 10.6491(1), and c = 8.8578(1) Å (Figures 5a and S14). This polymorph is denoted β-$K_2B_{12}(OH)_{12}$. The second order transition is clearly seen from the sequential refinement of the unit cell parameters as a function of temperature (Figures 4b & 4c). Notably, the merging Bragg peaks start exhibiting peak broadening, indicating directional disorder in the crystal structure. This anisotropic peak broadening was modelled by individual peak shapes for the significantly broadened peaks. No clear trend for the (hkl) values was found, thus the nature of the disorder is unknown.

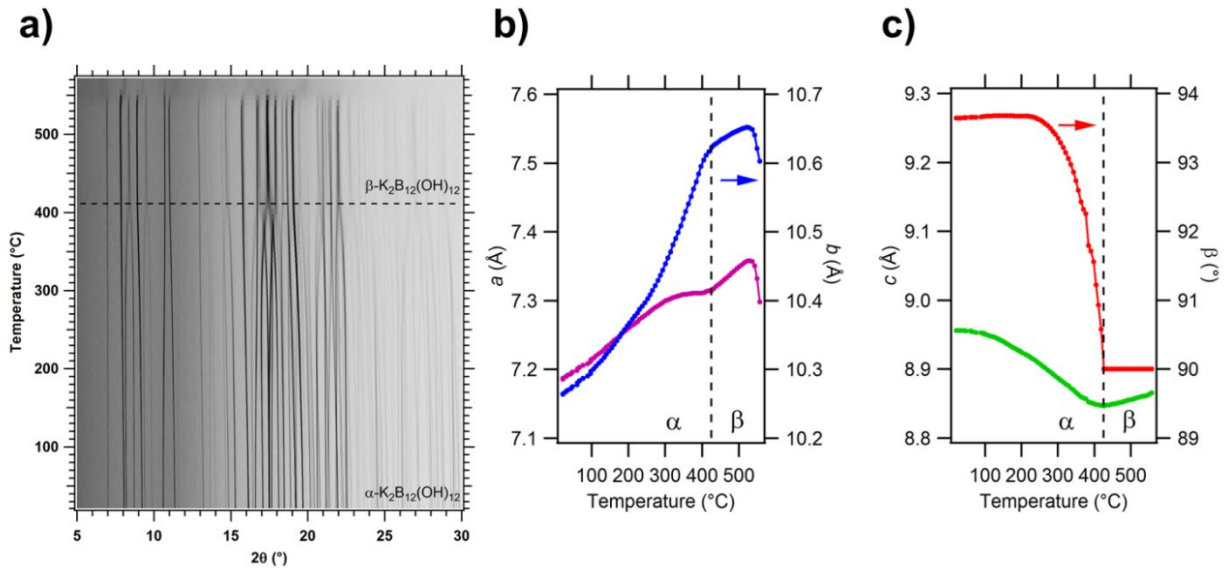

Figure 4: (a) *In-situ* synchrotron radiation powder X-ray diffraction of $K_2B_{12}(OH)_{12}$ (K1) heated from RT to 570 °C ($\Delta T/\Delta t$ = 5 °C/min, λ = 0.8263076 Å); (b,c) Lattice parameters of $K_2B_{12}(OH)_{12}$ refined from *in-situ* synchrotron X-ray diffraction data and the unit cell volume is plotted in Figure S15.

During the α-β transition only minor changes occur to the anion sublattice, as one might expect from the second order nature. In the α-polymorph, the anion sublattice can be considered a distorted face centered lattice with lattice parameters a = 11.115(7), b = 10.240(9), c = 11.837(8) Å, and β = 102.752(4)°, while the sublattice in the β-polymorph has lattice parameters a = c = 11.5413, b = 10.6744 Å, and β = 100.585°. The slight shift in the sublattice is likely a result of a change in the K^+ coordination environment, as the K−O coordination number increases from seven to nine. In order to understand the driving force of this rearrangement, the intermolecular interactions were further investigated. In the α-polymorph the presence of hydrogen bonds are clear from O−O distances as short as ~2.76 Å,[28] which is significantly shorter than the combined van der Waals radius of 3.04 Å, indicating a positive interaction. On the other hand, the β-

polymorph exhibits a minimum O–O distance of ~2.95 Å, much closer to the combined van der Waals radius. This suggests that the hydrogen bonds are significantly weakened or broken upon heating, which is in part compensated by a stronger interaction between the anion and K^+ via a higher K−O coordination number, from 7 to 9. Thus, the phase transition may, in part, be driven by the entropy gain of freeing hydrogen from the directional bond to a neighboring oxygen.

The increase in the number of oxygen atoms coordinating potassium in the β-polymorph results in an increase in the K–K distance with the shortest being 3.803(3) Å compared to 3.543(3) Å for α-$K_2B_{12}(OH)_{12}$,[28] while the K−O distances after the transition range from 2.823(3) - 3.163(3) Å. The K–O and K–K distances are close to the range previously shown for $[KO_9]$ in $K_2ZnSi_2O_6$ of 2.751(2) – 3.305(3) Å and 3.657(2) – 3.899(2) Å, respectively.[30] Viewing the structure of β-$K_2B_{12}(OH)_{12}$ along the *a*-axis reveals that all K^+ are linked in a polymeric structure via oxygen atoms (Figure 5b,c), forming alternating columns of $[KO_9]$ and $[B_{12}(OH)_{12}]^{2-}$, similar to the α-polymorph. In β-$K_2B_{12}(OH)_{12}$, the $[KO_9]$ tricapped trigonal polyhedra are interconnected via alternating face and edge sharing interactions (Figure 5c), whereas only edge sharing connections between $[KO_7]$ polyhedra are observed in α-$K_2B_{12}(OH)_{12}$.

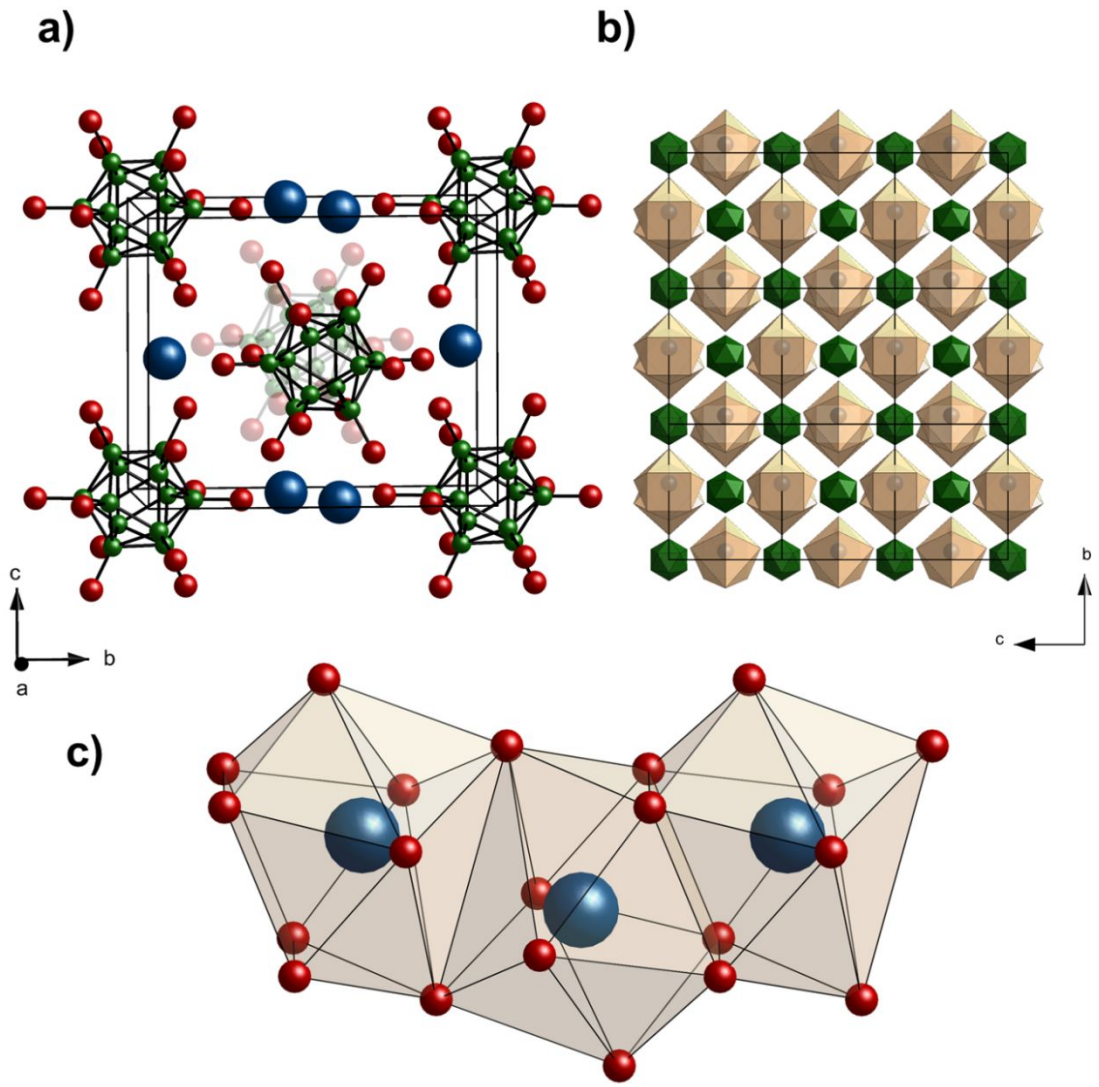

Figure 5: Representative views of β-$K_2B_{12}(OH)_{12}$. (a) Crystal structure of β-$K_2B_{12}(OH)_{12}$; (b) Crystal packing of β-$K_2B_{12}(OH)_{12}$ as seen along the *a*-axis; (c) Geometry of [KO_9] polyhedra, showing edge and face sharing. K atoms are shown as blue spheres; O atoms as red spheres; B as green spheres; $[B_{12}(OH)_{12}]^{2-}$ is represented with as green polyhedra and [KO_9] polyhedra represented with light brown faces. Hydrogen atoms were not modelled and are thus not shown.

Cesium hydroxylated closo-dodecaborate

In-situ SR-PXD data of Cs1 at RT reveal reflections from the known α-$Cs_2B_{12}(OH)_{12}\cdot 2H_2O$ structure[28] as well as a hitherto unidentified second polymorph of $Cs_2B_{12}(OH)_{12}\cdot 2H_2O$, denoted β-$Cs_2B_{12}(OH)_{12}\cdot 2H_2O$ (Figures 6, S1 and S16). The two polymorphs exist in an approximately 1:1 ratio at RT, however, upon heating, the relative amount of the β-polymorph increases slightly (55.5(2) wt% at RT to 57.7(5) wt% at 111 °C). In the structure of α-$Cs_2B_{12}(OH)_{12}\cdot 2H_2O$ the anions pack in hexagonal layers along the *c*-axis in an AAA sequence, slightly misaligned due to the β-angle being different from 90° (Figure 7a), which is reminiscent of the anion packing observed in $Na_2B_{12}H_{12}\cdot 2NH_3$.[31] The anion layers are held together by parallel 1D-cation chains, in which the cations coordinate approximately trigonally to the anions above and below, as well as to two H_2O in the plane. Each H_2O is shared by two Cs^+, forming two identical Cs-O-Cs chains along the *b*-axis. Similarities between the α- and β-polymorphs are already evident from the unit cell parameters (Table 2), which are almost identical apart from the *a*-axis which is approximately doubled in the β-polymorph. The longer *a*-axis is explained by a distortion of the hexagonal layers resulting in a disruption of every other Cs-O-Cs chain (Figure 7b), or vice versa. In the disrupted chains the H_2O molecules are no longer shared between two Cs^+, leading to longer and more irregular Cs−Cs distances of 4.319(4) and 5.198(3) Å, compared to 3.875(3) Å in the undisrupted chain.

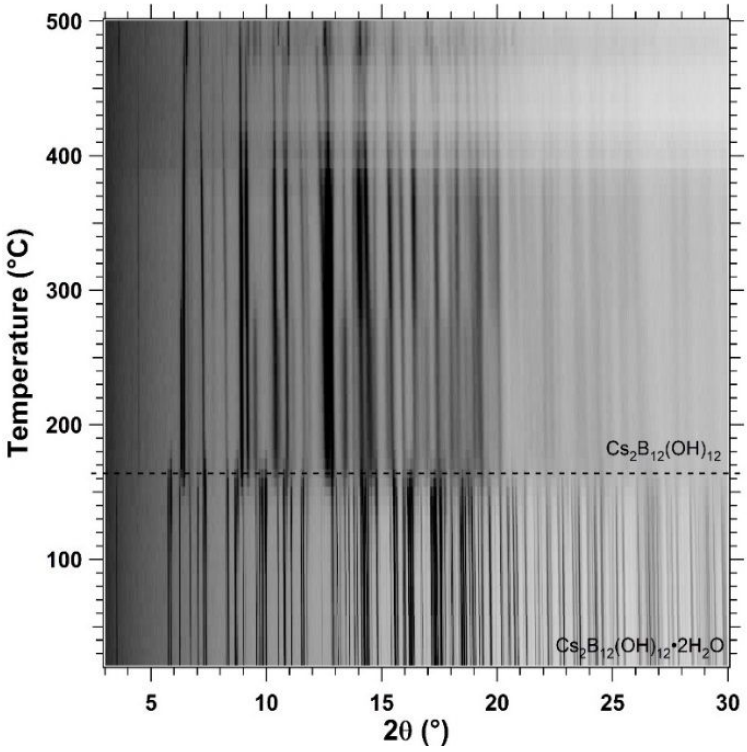

Figure 6: *In-situ* synchrotron radiation powder X-ray diffraction of $Cs_2B_{12}(OH)_{12}$ (Cs1) heated from RT to 500 °C ($\Delta T/\Delta t$ = 5 °C/min, λ = 0.8263076Å).

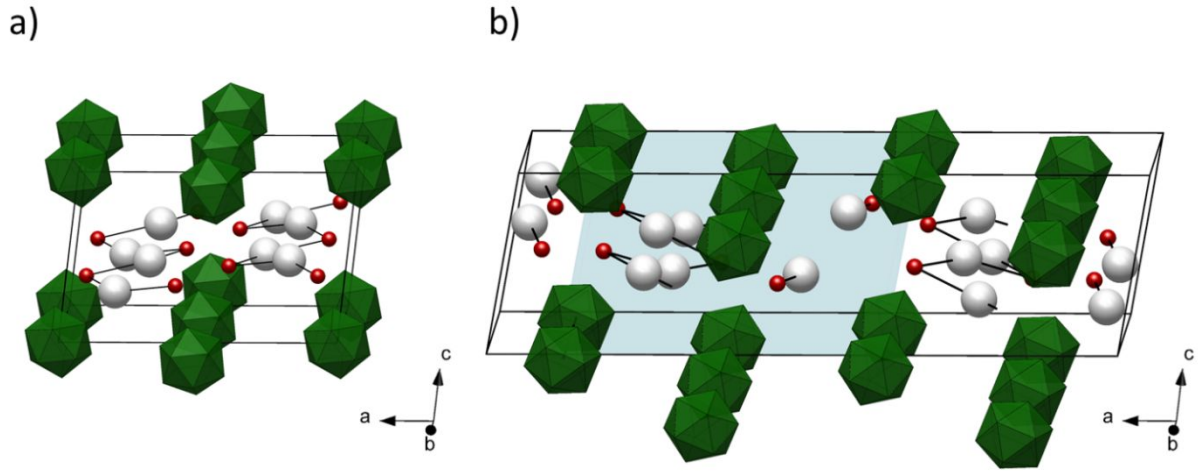

Figure 7: Comparison of the crystal structures of (a) α-$Cs_2B_{12}(OH)_{12}\cdot 2H_2O$ and (b) β-$Cs_2B_{12}(OH)_{12}\cdot 2H_2O$ showing the distortion of the hexagonal layers and breaking of alternating Cs-

O-Cs chains. The blue shadow highlights the similarity between the two structures. H and OH have been omitted for clarity. Green dodecahedron: B_{12} cage; red: O; white: Cs.

At ~100 °C a new set of diffraction peaks emerges as the intensity of the peaks belonging to the two dihydrates starts to decrease (Figure S17). A significant peak overlap and low intensity of the new peaks meant that the peaks could not reliably be indexed, though an orthorhombic unit cell with a reasonable volume did describe the peaks that could be identified. The lattice parameters are a = 8.046, b = 9.758, and c = 19.482 Å (not refined), resulting in a V/Z of 382.4 Å^3 compared to 399.1 Å^3 for α-$Cs_2B_{12}(OH)_{12}\cdot 2H_2O$, which indicates that it could be a monohydrate complex. The new peaks disappear along with the peaks from the two dihydrates at around 170 °C, forming $Cs_2B_{12}(OH)_{12}$. The crystal structure of $Cs_2B_{12}(OH)_{12}$ could not be solved or indexed due to significant peak broadening, peak overlap and the presence of at least two different sets of peaks, possibly due to polymorphism or impurities. At ~280 °C a subset of the new peaks disappears and finally at 470 °C the peaks of the main phase start fading and a new set of peaks emerge. Indexing of these reflections was unsuccessful in both cases because of the poor crystallinity of the samples. In an attempt to increase crystallinity, a sample was annealed at 300 °C for one week under an argon atmosphere, however, this resulted in amorphization of the sample, which had changed color from white to brown. Based on the TGA and MS results (Figures S8d and S13d) this is likely, to some extent, due to decomposition of the sample, however, based on *in-situ* SR-PXD, the sample is expected to be crystalline to at least 500 °C. It is possible that the amorphization process is slower than the timescale of the PXD experiment and/or that the closed atmosphere of the capillary during PXD (sealed by vacuum grease) slows or halts this process relative to the flowing Ar atmosphere of the TG. Interestingly, this trend is observed for all four samples. TG-DSC-MS analysis (Figures S8 and S13) reveals a mass loss, as

water, and in some cases hydrogen, is released at temperatures significantly lower than the decomposition temperature from *in-situ* SR-PXD.

Table 2: Crystallographic data for $M_2B_{12}(OH)_{12}$ obtained by Rietveld refinement of SR-PXD data or from literature data.

Compound	SG	Parameters	Reference
Li			
$Li_2B_{12}(OH)_{12}·H_2O$	Unknown	-	-
α-$Li_2B_{12}(OH)_{12}$	Unknown	-	This work
β-$Li_2B_{12}(OH)_{12}$	Tetragonal/	a = 12.087(2) Å	This work
	Orthorhombic	b = 12.087(3) Å	
		c = 8.516(2) Å	
		V/Z = 311.0(1) Å^3	
γ-$Li_2B_{12}(OH)_{12}$	Cubic	a = 8.5707(2) Å	This work
	Im-3	V/Z = 314.8(2) Å^3	
Na			
$Na_2B_{12}(OH)_{12}·4H_2O$	Triclinic	a = 8.55(1) Å	[28]
	P-1	b = 8.66(1) Å	
		c = 12.16(2) Å	
		α = 69.55(2)°	
		β = 80.13(2)°	
		γ = 75.67(2)°	
		V/Z = 407.5 Å^3	
α-$Na_2B_{12}(OH)_{12}$	Unknown	-	This work
β-$Na_2B_{12}(OH)_{12}$	Cubic	a = 8.6291(3) Å	This work
	Im-3	V/Z = 321.26(2) Å^3	
K			
α-$K_2B_{12}(OH)_{12}$	Monoclinic	a = 7.18531(4) Å	[28]

	$P2_1/n$	b = 10.26298(5) Å	
		c = 8.95575(4) Å	
		β = 93.6430(3)°	
		V/Z = 329.55(1) Å^3	
β-$K_2B_{12}(OH)_{12}$	Orthorhombic	a = 7.3559(1) Å	This work
	$Pnnm$	b = 10.6491(1) Å	
		c = 8.8578(1) Å	
		V/Z = 346.93(1) Å^3	
Cs			
α-$Cs_2B_{12}(OH)_{12}\cdot 2H_2O$	Monoclinic	a = 13.1251(1) Å	[28]
	$P2_1/a$	b = 7.34495(6) Å	
		c = 8.29106(7) Å	
		β = 97.4071(1)°	
		V/Z = 396.31(3) Å^3	
β-$Cs_2B_{12}(OH)_{12}\cdot 2H_2O$	Monoclinic	a = 27.3572(2) Å	This Work
	$P2_1/a$	b = 7.29938(6) Å	
		c = 8.20572(6) Å	
		β = 100.8225(5)°	
		V/Z = 402.37(4) Å^3	
$Cs_2B_{12}(OH)_{12}$	Unknown	-	This work

Ionic conductivity

The ionic conductivities (σ) of the four $M_2B_{12}(OH)_{12}$ compounds are generally low (Figure 8), especially for M = Na, K, Cs, while $Li_2B_{12}(OH)_{12}$ shows conductivities close to that of the low temperature polymorph of $Na_2B_{12}H_{12}$ (on the first heating ramp). While the conductivity of $Li_2B_{12}(OH)_{12}$ does not show a sudden order of magnitude increase, such as for $Na_2B_{12}H_{12}$, the conductivity nevertheless reaches technologically relevant values of $2.2\cdot10^{-2}$ S cm^{-1} at 375 °C,

significantly higher than the perhalogenated compounds with similarly bulky substituents. On the other hand, $Na_2B_{12}(OH)_{12}$ shows markedly lower conductivities compared to $Na_2B_{12}H_{12}$, as well as $Na_2B_{12}Cl_{12}$ at $T < 300$ °C. However, compared to the Li analogue there are clear signs of the order-disorder transition at around 300 °C where the conductivity increases abruptly, though it is not as pronounced as for other *closo*-borates such as $Na_2B_{12}H_{12}$. This is likely because of the lack of significant anion disorder, which is otherwise usually observed along with the on-set of cation disorder in other *closo*-borates and derivatives. Above the phase transition of $Na_2B_{12}(OH)_{12}$ the ionic conductivity exceeds those of the perhalogenated compounds, however, at elevated temperature the ionic conductivity of $Na_2B_{12}(OH)_{12}$ starts decreasing, which is suggested to be correlated with the decomposition of the compound, based on TGA/DSC (Figures S8b and S12). Interestingly, similar effects are not observed for the other compounds, despite a clear mass loss observed from TGA measurements (Figure S8).

As mentioned, an explanation for the relatively low conductivities may be found in the lack of significant anion disorder. While the presence of hydrogen bonds among the anions could be responsible for a lack of a fully disordered polymorph at RT, the analysis of the crystal structures of the high temperature polymorphs suggests that these bonds are significantly weakened or even broken at elevated temperature. Thus, the interaction between the cation and anion may instead explain the lack of anion disorder. This interaction is expected to be stronger and more directional compared to the hydrogenous analogues $[B_{12}H_{12}]^{2-}$, and stronger than the monovalent carbaborates $[CB_{11}H_{12}]^{-}$, owing to the negative partial charge of the oxygen. Such negatively charged groups on the boron cage have previously been suggested to create deep potential wells for the cation, resulting in an increase of the order-disorder transition temperature.[22,32]

The activation energies for ionic conduction were calculated based on the relation $\ln(\sigma T) = \ln(A) - E_a/(k_b T)$ and can be found in Figure 8. The values are generally relatively high but compare well with the value of $Na_2B_{12}H_{12}$ (~0.87 eV estimated from data extracted from a previous study based on the linear region between 140 - 220 °C (Figure 8)). $Na_2B_{12}(OH)_{12}$ shows the highest value of 1.04 eV, which may explain the significant difference in the ionic conductivity between the Li and Na compound. However, even in the disordered phase of $Na_2B_{12}(OH)_{12}$ where the activation energy is expected to decrease significantly, the conductivity of the Li analogue remains superior.

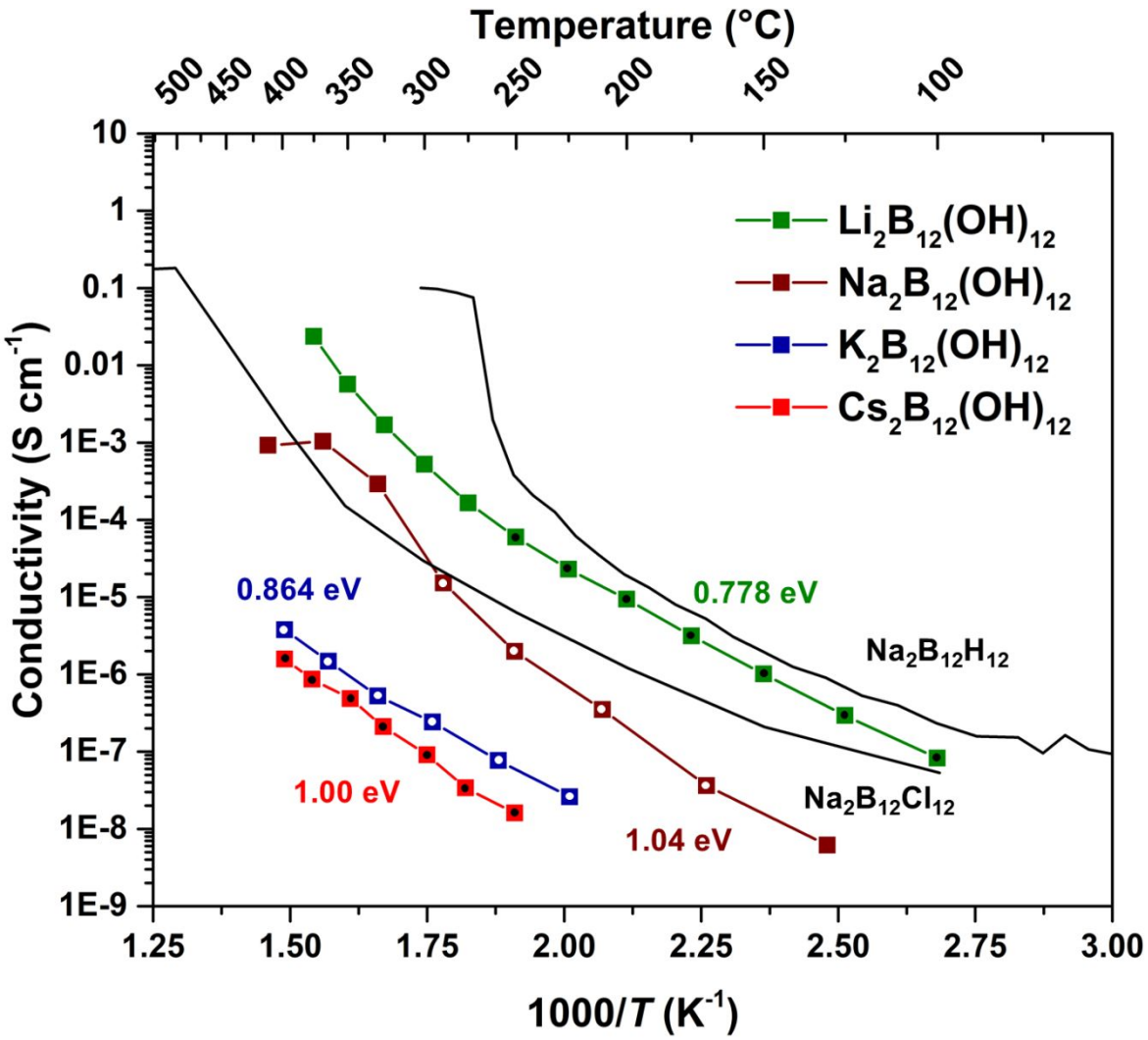

Figure 8: Ionic conductivity of Li2 (green line), Na2 (red line), K1 (magenta line) and Cs2 (blue line) as a function of temperature, compared with $Na_2B_{12}H_{12}$ (first heating ramp), and $Na_2B_{12}Cl_{12}$.[22,33] The colored values represent the apparent activation energy of the respective compound, based on the data points marked with a dot.

Conclusion

The compounds $Li_2B_{12}(OH)_{12}$, $Na_2B_{12}(OH)_{12}$, $K_2B_{12}(OH)_{12}$, and $Cs_2B_{12}(OH)_{12}$ have been prepared from $Cs_2B_{12}H_{12}$ and studied with *in-situ* SR-PXD, FTIR, DSC-TGA, MS, and EIS. The

in-situ SR-PXD data reveal the removal of water from the crystal structure of $Li_2B_{12}(OH)_{12}$, $Na_2B_{12}(OH)_{12}$, and $Cs_2B_{12}(OH)_{12}$, which is confirmed by the FTIR measurements. *In-situ* SR-PXD data also reveal thermal polymorphism of $Li_2B_{12}(OH)_{12}$, $Na_2B_{12}(OH)_{12}$, and $K_2B_{12}(OH)_{12}$, showing evidence of hydrogen bond weakening/breaking upon heating, as well as the introduction of a disordered cation sublattice in the case of Li and Na. The ionic conductivity of all of the samples are lower than the comparable compound $Na_2B_{12}H_{12}$. This is suggested to be due to the lack of a disordered anion sublattice, otherwise observed for most *closo*-borates, which may be a result of relatively strong and directional anion-cation interactions. In light of this, for symmetric anions, substitutions on the boron cage should likely be restricted to close to neutral or partially positive groups, such as for $[B_{12}H_{12}]^{2-}$.[18] It is possible that cation substitution to form dual cationic compounds, e.g. $LiNaB_{12}(OH)_{12}$, could tune the ion conductivity in a similar manner to $LiNaB_{12}H_{12}$.[34]

Supporting Information. PXD data of as-synthesized materials. FTIR data of dehydrated samples. TGA-DSC-MS data. *In-situ* SR-PXD of Li1. Comparisons of crystal structure models with measured PXD data. Tables of EIS data and results.

Corresponding Author

* Mark Paskevicius: m.paskevicius@curtin.edu.au, +61 9266 7248

* Torben R. Jensen: trj@chem.au.dk, +45 2272 1486

Author Contributions

The manuscript was written through contributions of all authors. All authors have given approval to the final version of the manuscript.

Mark Paskevicius thanks the Australian Research Council (ARC) for a Future Fellowship (FT160100303). Part of this research was undertaken on the Powder Diffraction beamline at the Australian Synchrotron, part of ANSTO. This work was also supported by the Danish Council for Independent Research (HyNanoBorN, DFF – 4181-00462 and SOS-MagBat DFF - 9041-00226B), Center for Materials Crystallography (DNRF93), The Danish Research Council for Nature and Universe (DanScatt), the Carlsberg Foundation, and NordForsk via the project Functional Hydrides - FunHy.

(1) Kong, L.; Li, C.; Jiang, J.; Pecht, M. Li-Ion Battery Fire Hazards and Safety Strategies. *Energies* **2018**, *11*, 2191.

(2) Greenwood, N. N.; Earnshaw, A. *Chemistry of the Elements*, 2nd Edition; Elsevier, 1997.

(3) Hansen, B. R. S.; Paskevicius, M.; Li, H.; Akiba, E.; Jensen, T. R. Metal Boranes: Progress and Applications. *Coord. Chem. Rev.* **2016**, *323*, 60–70.

(4) Zheng, F.; Kotobuki, M.; Song, S.; Lai, M. O.; Lu, L. Review on Solid Electrolytes for All-Solid-State Lithium-Ion Batteries. *J. Power Sources* **2018**, *389*, 198–213.

(5) Kamaya, N.; Homma, K.; Yamakawa, Y.; Hirayama, M.; Kanno, R.; Yonemura, M.; Kamiyama, T.; Kato, Y.; Hama, S.; Kawamoto, K.; Mitsui, A. A Lithium Superionic Conductor. *Nat. Mater.* **2011**, *10*, 682–686.

(6) Thangadurai, V.; Narayanan, S.; Pinzaru, D. Garnet-Type Solid-State Fast Li Ion Conductors for Li Batteries: Critical Review. *Chem. Soc. Rev.* **2014**, *43*, 4714.

(7) Hayashi, A.; Noi, K.; Sakuda, A.; Tatsumisago, M. Superionic Glass-Ceramic Electrolytes for Room-Temperature Rechargeable Sodium Batteries. *Nat. Commun.* **2012**, *3*, 856.

(8) Yuan, H.; Li, H.; Zhang, T.; Li, G.; He, T.; Du, F.; Feng, S. A $K_2Fe_4O_7$ Superionic Conductor for All-Solid-State Potassium Metal Batteries. *J. Mater. Chem. A* **2018**, *6*, 8413-8418.

(9) Ley, M. B.; Boulineau, S.; Janot, R.; Filinchuk, Y.; Jensen, T. R. New Li Ion Conductors and Solid State Hydrogen Storage Materials: $LiM(BH_4)_3Cl$, M = La, Gd. *J. Phys. Chem. C* **2012**, *116*, 21267–21276.

(10) Ley, M. B.; Ravnsbæk, D. B.; Filinchuk, Y.; Lee, Y.-S.; Janot, R.; Cho, Y. W.; Skibsted, J.; Jensen, T. R. $LiCe(BH_4)_3Cl$, a New Lithium-Ion Conductor and Hydrogen Storage Material with Isolated Tetranuclear Anionic Clusters. *Chem. Mater.* **2012**, *24*, 1654–1663.

(11) Ley, M. B.; Jørgensen, M.; Černý, R.; Filinchuk, Y.; Jensen, T. R. From $M(BH_4)_3$ (M = La, Ce) Borohydride Frameworks to Controllable Synthesis of Porous Hydrides and Ion Conductors. *Inorg. Chem.* **2016**, *55*, 9748–9756.

(12) Matsuo, M.; Nakamori, Y.; Orimo, S. I.; Maekawa, H.; Takamura, H. Lithium Superionic Conduction in Lithium Borohydride Accompanied by Structural Transition. *Appl. Phys. Lett.* **2007**, *91*, 1–4.

(13) Kim, S.; Oguchi, H.; Toyama, N.; Sato, T.; Takagi, S.; Otomo, T.; Arunkumar, D.; Kuwata, N.; Kawamura, J.; Orimo, S. A Complex Hydride Lithium Superionic Conductor for High-Energy-Density All-Solid-State Lithium Metal Batteries. *Nat. Commun.* **2019**, *10*, 1081.

(14) Hirscher, M.; Yartys, V. A.; Baricco, M.; Bellosta von Colbe, J.; Blanchard, D.; Bowman, R. C.; Broom, D. P.; Buckley, C. E.; Chang, F.; Chen, P.; Cho, Y. W.; Crivello, J.-C.; Cuevas, F.; David, W. I. F.; de Jongh, P. E.; Denys, R. V.; Dornheim, M.; Felderhoff, M.; Filinchuk, Y.; Froudakis, G. E.; Grant, D. M.; Gray, E. M.; Hauback, B. C.; He, T.; Humphries, T. D.; Jensen, T. R.; Kim, S.; Kojima, Y.; Latroche, M.; Li, H.-W.; Lototskyy, M. V.; Makepeace, J. W.; Møller, K. T.; Naheed, L.; Ngene, P.; Noréus, D.; Nygård, M. M.; Orimo, S.; Paskevicius, M.; Pasquini, L.; Ravnsbæk, D. B.; Veronica Sofianos, M.; Udovic, T. J.; Vegge, T.; Walker, G. S.; Webb, C. J.; Weidenthaler, C.; Zlotea, C. Materials for Hydrogen-Based Energy Storage – Past, Recent Progress and Future Outlook. *J. Alloys Compd.* **2020**, *827*, 153548.

(15) Latroche, M.; Blanchard, D.; Cuevas, F.; El Kharbachi, A.; Hauback, B. C.; Jensen, T. R.; de Jongh, P. E.; Kim, S.; Nazer, N. S.; Ngene, P.; Orimo, S.; Ravnsbæk, D. B.; Yartys, V. A. Full-Cell Hydride-Based Solid-State Li Batteries for Energy Storage. *Int. J. Hydrogen Energy* **2019**, *44*, 7875–7887.

(16) Yan, Y.; Grinderslev, J. B.; Lee, Y.; Jørgensen, M.; Cho, Y. W.; Černý, R.; Jensen, T. R. Ammonia-Assisted Fast Li-Ion Conductivity in a New Hemiammine Lithium Borohydride, $LiBH_4 \cdot 1/2NH_3$. *Chem. Commun.* **2020**, *6174*, 2–5.

(17) Yan, Y.; Dononelli, W.; Jørgensen, M.; Grinderslev, J.; Lee, Y.-S.; Cho, Y. W.; Černỳ, R.; Hammer, B.; Jensen, T. R. The Mechanism of Mg^{2+} Conductivity in Ammine Magnesium Borohydride Promoted by a Neutral Molecule. *Phys. Chem. Chem. Phys.* **2020**, *Accepted*. https://doi.org/10.1039/D0CP00158A

(18) Tang, W. S.; Unemoto, A.; Zhou, W.; Stavila, V.; Matsuo, M.; Wu, H.; Orimo, S.; Udovic, T. J. Unparalleled Lithium and Sodium Superionic Conduction in Solid Electrolytes with Large Monovalent Cage-like Anions. *Energy Environ. Sci.* **2015**, *8*, 3637–3645.

(19) Paskevicius, M.; Hansen, B. R. S.; Jørgensen, M.; Richter, B.; Jensen, T. R. Multifunctionality of Silver Closo-Boranes. *Nat. Commun.* **2017**, *8*, 15136.

(20) Pitochelli, A. R.; Hawthorne, F. M. The Isolation of the Icosahedral $B_{12}H_{12}^{-2}$ Ion. *J. Am. Chem. Soc.* **1960**, *82*, 3228–3229.

(21) Udovic, T. J.; Matsuo, M.; Unemoto, A.; Verdal, N.; Stavila, V.; Skripov, A. V; Rush, J. J.; Takamura, H.; Orimo, S. Sodium Superionic Conduction in $Na_2B_{12}H_{12}$. *Chem. Commun.* **2014**, *50*, 3750–3752.

(22) Hansen, B. R. S.; Paskevicius, M.; Jørgensen, M.; Jensen, T. R. Halogenated Sodium-*Closo*-Dodecaboranes as Solid-State Ion Conductors. *Chem. Mater.* **2017**, *29*, 3423–3430.

(23) Bukovsky, E. V; Peryshkov, D. V; Wu, H.; Zhou, W.; Tang, W. S.; Jones, W. M.; Stavila, V.; Udovic, T. J.; Strauss, S. H. Comparison of the Coordination of $B_{12}F_{12}^{2-}$, $B_{12}Cl_{12}^{2-}$, and $B_{12}H_{12}^{2-}$ to Na^+ in the Solid State: Crystal Structures and Thermal Behavior of $Na_2(B_{12}F_{12})$, $Na_2(H_2O)_4(B_{12}F_{12})$, $Na_2(B_{12}Cl_{12})$, and $Na_2(H_2O)_6(B_{12}Cl_{12})$. *Inorg. Chem.* **2017**, *56*, 4369–4379.

(24) Tang, W. S.; Matsuo, M.; Wu, H.; Stavila, V.; Zhou, W.; Talin, A. A.; Soloninin, A. V.; Skoryunov, R. V.; Babanova, O. A.; Skripov, A. V.; Unemoto, A.; Orimo, S.-I.; Udovic, T. J. Liquid-Like Ionic Conduction in Solid Lithium and Sodium Monocarba-*Closo*-Decaborates Near or at Room Temperature. *Adv. Energy Mater.* **2016**, *6*, 1502237.

(25) Bayer, M. J.; Hawthorne, M. F. An Improved Method for the Synthesis of [*Closo*-$B_{12}(OH)_{12}]^{-2}$. *Inorg. Chem.* **2004**, *43*, 2018–2020.

(26) Dyadkin, V.; Pattison, P.; Dmitriev, V.; Chernyshov, D. A New Multipurpose Diffractometer PILATUS@SNBL. *J. Synchrotron Radiat.* **2016**, *23*, 825–829.

(27) Favre-Nicolin, V.; Černý, R. FOX, "Free Objects for Crystallography": A Modular Approach to Ab Initio Structure Determination from Powder Diffraction. *J. Appl. Crystallogr.* **2002**, *35*, 734–743.

(28) Peymann, T.; Knobler, C. B.; Khan, S. I.; Hawthorne, M. F. Dodecahydroxy-*Closo*-Dodecaborate(2−). *J. Am. Chem. Soc.* **2001**, *123*, 2182–2185.

(29) Rodríguez-Carvajal, J. Recent Advances in Magnetic Structure Determination by Neutron Powder Diffraction. *Phys. B Condens. Matter* **1993**, *192*, 55–69.

(30) Hogrefe, A. R.; Czank, M. Synthetic Dipotassium Zinc Disilicate. *Acta Crystallogr. Sect. C Cryst. Struct. Commun.* **1995**, *51*, 1728–1730.

(31) Hansen, B. R. S.; Tumanov, N.; Santoru, A.; Pistidda, C.; Bednarcik, J.; Klassen, T.; Dornheim, M.; Filinchuk, Y.; Jensen, T. R. Synthesis, Structures and Thermal Decomposition of Ammine $M_xB_{12}H_{12}$ Complexes (M = Li, Na, Ca). *Dalt. Trans.* **2017**, *46*, 7770–7781.

(32) Jørgensen, M.; Shea, P. T.; Tomich, A. W.; Varley, J. B.; Bercx, M.; Lovera, S.; Černý, R.; Zhou, W.; Udovic, T. J.; Lavallo, V.; Jensen, T. R.; Wood, B. C.; Stavila, V. Understanding Superionic Conductivity in Lithium and Sodium Salts of Weakly Coordinating *Closo*-Hexahalocarbaborate Anions. *Chem. Mater.* **2020**, *32*, 1475–1487.

(33) Udovic, T. J.; Matsuo, M.; Unemoto, A.; Verdal, N.; Stavila, V.; Skripov, A. V.; Rush, J. J.; Takamura, H.; Orimo, S. I. Sodium Superionic Conduction in $Na_2B_{12}H_{12}$. *Chem. Commun.* **2014**, *50*, 3750–3752.

(34) He, L.; Li, H.-W.; Nakajima, H.; Tumanov, N.; Filinchuk, Y.; Hwang, S.-J.; Sharma, M.; Hagemann, H.; Akiba, E. Synthesis of a Bimetallic Dodecaborate LiNaB12H12 with Outstanding Superionic Conductivity. *Chem. Mater.* **2015**, 27, 5483-5486.

Table of Contents Image